# Simulation of optical spectra of $Eu^{3+}$ ion in fluorozirconate glasses by molecular dynamics simulation and point charge crystal field

Kohei Soga,[a] Hiroyuki Inoue, and Akio Makishima
*Department of Materials Engineering, School of Engineering, University of Tokyo, 7-3-1 Hongo, Bunkyo-ku, Tokyo 113-8656, Japan*

(Received 22 February 2000; accepted for publication 21 December 2000)

$Eu^{3+}$-doped fluorozirconate glasses with two compositions Zr:Ba=1:1(ZB11) and Zr:Ba =3:1(ZB31) were prepared. The emission, excitation, and fluorescence line narrowing spectra of those glasses were measured. Certain differences between the two glasses were observed in the observed spectra. Structural models of the glasses were simulated by molecular dynamics (MD) simulation. The optical spectra of $Eu^{3+}$ in those glasses were simulated from the simulated glass structures using a point charge crystal field. The differences in spectral characteristics between the two glasses in the observed spectra were reproduced in the simulated spectra. The MD simulation showed that the barium ions were more apt to coordinate to $EuF_a$ clusters than the zirconium ions were. © *2001 American Institute of Physics.* [DOI: 10.1063/1.1351542]

## I. INTRODUCTION

Rare-earth (RE) doped glasses are known as materials for glass lasers, fiber lasers, upconversion lasers, and optical amplifiers.[1–4] In these applications, the excitation and the emission are due to transitions of $4f$ electronic states of trivalent RE ions. Energy levels and transition rates of $4f$ electronic states of RE ions in solids are dominated by the surrounding structure of RE ions.[4–6] Therefore, their optical properties, such as spectral band shape and quantum efficiencies, are host dependent.

For the design of these materials, appropriate methods for the analysis and the prediction of optical properties are important. In 1962, Judd and Ofelt[7,8] proposed an excellent method of treatment for analyzing absorption intensity and predicting emission intensity. A number of researchers combined the Judd–Ofelt analysis with lifetime measurements to calculate the transition rates.[1–4] However, in most cases, the effects of the variation of the spectral band shape were neglected. For laser operation of the RE doped glass, the spectral band shape is important because it directly dominates the quantum efficiency. For upconversion lasers, the spectral shapes are also important because excited state absorption and energy transfer processes are strongly dependent on the spectral shapes of transitions. In the field of optical amplification, the use of a wavelength division multiplexing (WDM) technique is inevitable. The knowledge of spectral band shapes is essential for the design of RE doped glasses for WDM optical amplifiers.[3] Thus the simulation of optical spectra of RE ions in glasses is crucial for the design of these materials.

In many studies of the optical properties of RE-doped glasses, the discussions are based on the composition, not on the glass structure.[1] As mentioned above, the energy level splitting and the transition rate of $4f$ electronic states in RE ions are affected by the environment of the ions. Therefore, studies of the relation between a glass structure and its optical properties are significant from the standpoint of both science and application. In recent years, we have investigated this subject by using fluorescence line narrowing (FLN) emission observations[9] and a spectral simulation using a point charge crystal field, in which the structures of glass were simulated by molecular dynamic (MD) simulation.[10]

Analysis of the spectra of RE-doped crystals has been intensively carried out since the 1950s. Simulation of the optical spectra from a structure model including energy level splitting and transition intensities was performed for $KY_3F_{10}$ by Pocher *et al.* in 1978.[11–13] They have published numerous papers on various kinds of crystals.[14–24] The simulation of a RE spectrum in glass was first carried out on silicate glass in 1976 by Brecher and Riseberg.[25] The authors considered only the structure of $EuO_x$ first coordination polyhedrons, in which the intensity calculation of transitions between Stalk levels was not included. The symmetry of the RE site was limited for the simplicity of computation. In the 1980s, there were several articles dealing with this method.[26–30] In the last decade, we and several other researchers have been studying the simulation of spectra including transition intensities and the effects of ions outside the first coordination shell without assuming any site symmetry.[31–36]

Fluorozirconate glass is a good host for the RE ions because the quantum efficiencies of the emission of RE ions are relatively high in this glass.[1] In addition, the flat gain spectrum of an Er-doped fiber amplifier made of fluorozirconate glass is desirable for the WDM operation.[3]

The purpose of this article is to study a method of the simulation of the optical spectra of RE ions in glass and investigate the environment of RE ions in glass. The simulation of spectra is based on structural models by MD simulation. Even and odd crystal field parameters are calculated from the structural models using a point charge crystal field for the calculation of energy level splitting and transition intensities, respectively. Electronic states of $Eu^{3+}$ ions in a

[a]Author to whom correspondence should be addressed; electronic mail: ksoga@attglobal.net

 

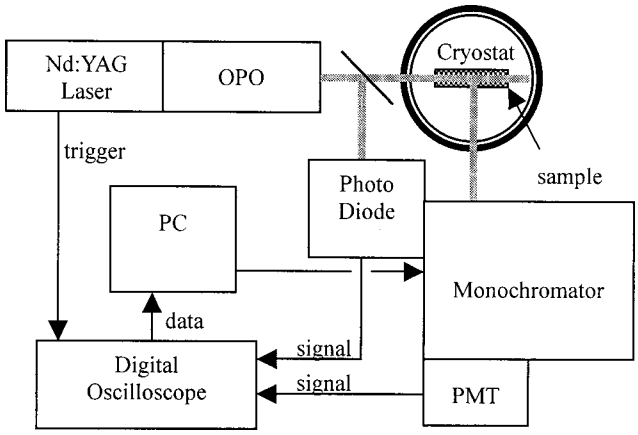


FIG. 1. Schematic diagram of FLN emission measurement system.

fluoride host were estimated by the DV-X$\alpha$ method for the simulation. Glasses with two different cation ratios were studied. By comparing the observed and the simulated spectra of the two glasses, the validity of the simulation method was obtained.

## II. EXPERIMENT

### A. Sample preparation

The compositions of the glass samples were $45ZrF_4 \cdot 45BaF_2 \cdot 4LaF_3 \cdot 4AlF_3 \cdot 2EuF_3$ (ZB11) and $67.5ZrF_4 \cdot 22.5BaF_2 \cdot 4LaF_3 \cdot 4AlF_3 \cdot 2EuF_3$ (ZB31). Glass batches for 10 g were prepared from commercially available fluorides (>99.9% purity). The batches were heated in a gold crucible using an electric furnace for 15 min at a temperature of 950 °C for ZB11 and at 850 °C for ZB31, respectively. The melts were pressed between aluminum blocks. The above processes were conducted in a $N_2$ glove box.

### B. Measurement of emission spectra

The schematic diagram for the FLN measurements is shown in Fig. 1. The concept and the method of measurement of FLN emission spectra have been described previously.[9,25] The system was calibrated using a standard lamp. The excitation wavelengths were 17 271–17 346 $cm^{-1}$ (corresponding to the excitation due to $^7F_0-^5D_0$ transition) with a 15 $cm^{-1}$ interval. The emission spectra were measured in the 13 698–17 241 $cm^{-1}$ range (corresponding to the emissions due to $^5D_0-^7F_1$, $^7F_2$, $^7F_3$, and $^7F_4$ transitions). Broadband emission spectra were calculated by integrating the FLN emission spectra.

## III. METHOD OF CALCULATION

### A. Molecular dynamics simulation

The method and potential parameters of MD simulations are described in Ref. 10. The compositions and cell sizes are shown in Table I. $LaF_3$ and $AlF_3$ were removed as minor components for the simplicity of the computation. Each cell contained two europium ions. To obtain the variation of the $Eu^{3+}$ sites in the glass structure, MD simulations were performed for 200 different sets of random initial coordinates. Thus 400 $Eu^{3+}$ sites were simulated for glass composition by MD simulation.

TABLE I. Cell size, number of atoms, and composition in a cell in MD simulation.

| Sample name | Cell size (Å) | Number of atoms | Composition |
|---|---|---|---|
| ZB11 | 18.04 | 392 | 48Zr–48Ba–2Eu–294F |
| ZB31 | 17.96 | 407 | 66Zr–23Ba–2Eu–316F |

### B. Energy level and transition intensity calculation of the 4f electrons in $Eu^{3+}$

A detailed method of the calculations can be found in the literature.[4,11–13] In this article, we describe briefly the key theoretical points for the calculation. Using a point charge approximation for the ions surrounding the rare earth, the Hamiltonian describing the electrostatic field (crystal field) at the europium ion can be written as

$$H_{\mathrm{CF}} = \sum_k \sum_{q=-k}^{k} B_{kq} C_{kq}, \tag{1}$$

$$B_{kq} = -a_k \frac{e^2}{4\pi\epsilon_0} \langle 4f|r^k|4f\rangle \sum_i \frac{Q_i}{r_i^{k+1}} C_{kq}^* = a_k \langle 4f|r^k|4f\rangle A_{kq}, \tag{2}$$

$$A_{kq} = -\frac{e^2}{4\pi\epsilon_0} \sum_i \frac{Q_i}{r_i^{k+1}} C_{kq}^*, \tag{3}$$

where the ligand $i$ of charge $Q_i$ is at a distance $r_i$ from a europium ion, $\langle 4f|r^k|4f\rangle$ is the radial integral for the $4f$ electrons. The value of $\langle 4f|r^k|4f\rangle$ was calculated using the DV-X$\alpha$ method as described below. $C_{kq}$ is a tensor operator given with spherical harmonic function $Y_{kq}$ as

$$C_{kq} = \sqrt{\frac{4\pi}{2k+1}} Y_{kq}. \tag{4}$$

Crystal field parameters $A_{kq}$ were calculated form the $Q_i$ and $r_i$ in the structural models by MD simulation. A crystal field parameter with an odd $k$ contributes to the transition intensities, and that with an even $k$ contributes to the energy level splitting of the RE spectra. No symmetry for the RE sites was assumed for this calculation. Although all of the ions in a solid should be included in the summation with $i$, this kind of treatment is impossible. In the actual calculation, the summations in Eqs. (2) and (3) were limited to the ions within 200 Å from a europium ion because the longer the distance from the center ion is, the less the contribution to a crystal field as seen in Eq. (2). The necessity of encountering ions farther from a europium ion than the first coordinated fluorine ions was discussed in Ref. 10. It is known that correction factor $a_k$ is needed for the interpretation of a structural model to an optical spectrum.[12] In this study, $a_k$ was treated as an adjustable parameter.

The Hamiltonian for the $4f$ electronic state can be described as

$$H = H_0 + H_{SO} + H_{CF}, \tag{5}$$

where $H_0 + H_{SO}$ is the free ion Hamiltonian calculated from $E_1 = 5573.0\ \mathrm{cm}^{-1}$, $E_2 = 26.708\ \mathrm{cm}^{-1}$, $E_3 = 557.39\ \mathrm{cm}^{-1}$, and $\zeta = 1326.0\ \mathrm{cm}^{-1}$.[37]

By diagonalizing the matrix with the element

$$\langle \alpha SLJM_J | H | \alpha' S'L'J'M'_J \rangle \tag{6}$$

for the 51$|SL\rangle$ states, 399$|SLJ\rangle$ states, and 1393$|SLJM_J\rangle$ states, energy level splitting was obtained as the eigenvalues $\epsilon$ and the eigenvectors $|\alpha SLJM_J\rangle$ were calculated as

$$|\alpha SLJM_J\rangle = \sum_{SLJM_J} C_{SLJM_J} |SLJM_J\rangle. \tag{7}$$

In this calculation of energy levels, the value $k$ was limited to 2, 4, and 6 for the selection rule.

The magnetic dipole transition intensities can be calculated as described in Refs. 4 and 12 using the resultant eigenvectors $|\alpha SLJM_J\rangle$ of the above diagonarization. They are not sensitive to the local environment of the $Eu^{3+}$ ion because they apparently do not involve crystal field parameters.

The intensity of transition by the electric dipole operator $P$ between the two states $|\alpha SLJM_J\rangle$ and $|\alpha' S'L'J'M'_J\rangle$ is described by the method developed by Judd and Ofelt with[4,7,8]

$$\begin{aligned}\langle \alpha SLJM_J | \boldsymbol{P} | \alpha' S'L'J'M'_J \rangle &= \sum_{SLJM_J} \sum_{S'L'J'M'_J} C_{SLJM_J} C_{S'L'J'M'_J} \\ &\times \sum_{\lambda,k,q} (-1)^{q+\rho} [\lambda] \begin{pmatrix} 1 & \lambda & k \\ \rho & -(q+\rho) & q \end{pmatrix} \\ &\times A_{kq} b_k \Xi_{k,\lambda} \langle SLJM_J | U^{\lambda}_{q+\rho} | S'L'J'M'_J \rangle, \end{aligned} \tag{8}$$

$$\Xi_{k,\lambda} = 2 \sum_{n,l} (-1)^{f+1} (2f+1)(2l+1) \begin{Bmatrix} 1 & \lambda & k \\ f & l & f \end{Bmatrix} \times \frac{\langle f \| C^{(l)} \| l \rangle \langle l \| C^{(k)} \| f \rangle \langle 4f | r | nl \rangle \langle nl | r^k | 4f \rangle}{\Delta E_{4f-nl}}, \tag{9}$$

where $b_k$ is the correction factor for $\Xi_{k\lambda}$, which is also treated as an adjustable parameter in this study. The $A_{kq}$ parameters are the crystal field parameters described as Eq. (3) and were calculated from MD structural models using a point charge crystal field. The values of $k$ in the calculation of electric dipole transition intensities are limited to 1, 3, 5, and 7 for the selection rule.

The electronic states of rare earth ions are included as $\langle 4f | r^k | 4f \rangle$ in Eq. (2) and $\epsilon_{nl}$, $|nl\rangle$ in Eq. (9). For the simulation of spectra, the $5d$ and $ng$ states were encountered as $|nl\rangle$ states. We applied an electronic state calculation called DV-X$\alpha$ for the electronic state of the $Eu^{3+}$ ion in a fluoride host $EuF_3$ crystal. The program SCAT for the computation was provided by Adachi *et al.*[38] For the calculation, the first coordination polyhedron, $EuF_x$ was used. The second neighbor ions were treated as point charges. The DV-X$\alpha$ calculation gave the results for $\langle 4f | r^k | 4f \rangle$, $\epsilon_{5d}$ and $|5d\rangle$. $\epsilon_{ng}$, and $|ng\rangle$ were estimated by using the approximation described in the literature.[39]

TABLE II. Contribution of crystal field parameters ($A_{kq}$) to energy level splittings and transition intensities.

| $^5D_0 \rightarrow$ Energy level splitting | $^7F_1$ $k=2$ | $^7F_2$ $k=2,4$ | $^7F_3$ $k=4,6$ | $^7F_4$ $k=4,6$ |
|---|---|---|---|---|
| Intensity | MDT[a] | EDT[b] $k=1,3$ $\lambda=2$ | (forbidden) | EDT $k=3,5$ $\lambda=4$ |

[a]MDT: Magnetic dipole transition.
[b]EDT: Electric dipole transition.

## IV. RESULTS AND DISCUSSION

### A. Simulation of optical spectra and phenomenological parameters, $a_k$ and $b_k$

The excitation and emission spectra of europium ions were simulated using transition energies and intensities calculated from MD structural models. Obtaining smooth spectra to compare with the observed ones, each transition line was assumed to have a Gaussian distribution with a FWHM of 15 $\mathrm{cm}^{-1}$ at the position of the transition energy and with the height of the transition intensity. A spectrum was simulated integrating those lines for all of the structural models that belonged to a category.

The phenomenological parameters $a_k$ and $b_k$ had to be determined to calculate the energy level splitting and transition intensities. Due to the selection rules, the contribution of a crystal field parameter to an energy level splitting or a transition intensity is roughly limited by the $k$ value as shown in Table II. The selection rules are strictly valid when $J$ mixing is not encountered. Although the calculated energy levels and transition intensities were affected by $J$ mixing to some extent, the effects were relatively small and it is adequate to use those rules for the determination of $a_k$ and $b_k$. We determined the $a_k$ and $b_k$ parameters using the differences of their contribution of the crystal fields to the simulated spectra by the $k$ values. For example, the energy level splitting of the $^7F_1$ state is affected only by $A_{2q}$. Comparing the observed and the simulated spectra, the $a_2$ value was determined. In the case of $^7F_2$ energy splitting, only the crystal field parameters $A_{kq}$ with $k=2$ and 4 affect the splitting. Using the $a_2$ value obtained above, we could determine the $a_4$ parameter by comparing the observed and simulated spectra of $^7F_2$. Finally, using the $a_2$, $a_4$ parameters determined above and the $^7F_4$ spectra, the $a_6$ parameter was determined. The $a_k$ and $b_k$ parameters are listed in Table III together with the parameters calculated for the $EuF_3$ crystal by the DV-X$\alpha$ electronic state calculation. In the intensity calculation, $A_{7q}$ parameters were omitted because their contributions to the transition bands in our observation were negligible.

### B. Broadband emission and excitation spectra

Figure 2 shows the observed (b) and simulated (a) broadband emission spectra. The simulated broadband spec-

TABLE III. Electronic state parameters $\langle f|r^k|f\rangle$ and $\Xi_{k\lambda}$ calculated for $EuF_3$ crystal by DV-X$\alpha$ electronic state calculation and phenomenological factors $a_k$ and $b_k$ for the simulations of spectra.

| | Unit | $k$ | $\lambda$ | $EuF_3$ crystal (by DV-X$\alpha$) | $a_k$, $b_k$ |
|---|---|---|---|---|---|
| $\langle f\|r^k\|f\rangle$ | ($Å^2$) | 2 | — | 0.26 | 0.59 |
| | ($Å^4$) | 4 | — | 0.16 | 2.2 |
| | ($Å^6$) | 6 | — | 0.21 | 4.3 |
| $\Xi_{k\lambda}$ | ($10^{-6}$ $cm^2$/erg) | 1 | 2 | −0.75 | 0.93 |
| | ($10^{-22}$ $cm^2$/erg) | 3 | 2 | 0.47 | 3.0 |
| | ($10^{-22}$ $cm^2$/erg) | 3 | 4 | 0.47 | |
| | ($10^{-38}$ $cm^2$/erg) | 5 | 4 | −0.37 | 5.2 |
| | ($10^{-38}$ $cm^2$/erg) | 5 | 6 | −0.80 | |
| | ($10^{-54}$ $cm^2$/erg) | 7 | 6 | 0.59 | — |

tra are obtained by integrating spectral lines over all of the structural models for each glass. In relation to the transition intensity, the $^5D_0-^7F_1$ bands mostly consist of magnetic dipole transitions, and those intensities are insensitive to the glass structure. The crystal field affects only the splitting of the energy levels. However, the $^5D_0-^7F_2$ bands mostly consist of electric dipole transitions, whose intensities are sensitively changed by the crystal field, i.e., glass structure. Transition intensity corresponds to the area of an emission band. To compare the intensity of the structure sensitive bands, all of the emission spectra on this article were normalized so that the areas of the $^5D_0-^7F_1$ bands would be constant.

In observed emission spectra, the characteristic differences between the ZB11 and ZB31 glasses were revealed as the sharper profile of the ZB31 glass on the high-energy side of the $^5D_0-^7F_2$ band and on the low energy side of the $^5D_0-^7F_4$ band compared to those of the ZB11 glass. The emission intensity, spectral shape, and the above differences between the two glasses were reproduced in the simulated spectra.

The simulated and observed excitation spectra are shown in Fig. 3. In both spectra, the energy of the high-energy edge of the band of the ZB31 glass was higher than that of the ZB11 glass. This difference was reproduced in the simulated spectra. The energy of the low-energy edge of the ZB31 glass in the simulated spectrum was higher than that of the ZB11 glass. However, this feature did not appear in the observed spectra. The reason is not clear. One possible reason for this mismatch of the observed and simulated spectra is the neglect of the phonon effects, such as phonon sidebands or thermalization.

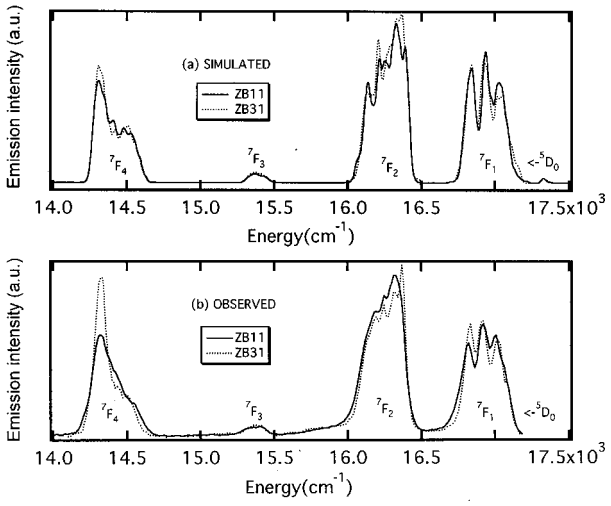


FIG. 2. Simulated (a) and observed (b) broadband emission spectra of $Eu^{3+}$ in ZB11 and ZB31 fluorozirconate glasses.

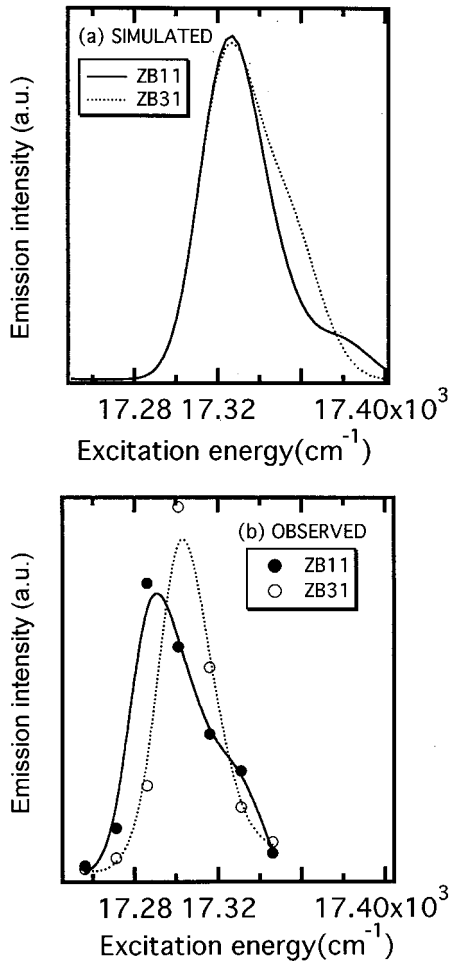


FIG. 3. Simulated (a) and observed (b) excitation spectra of $Eu^{3+}$ in ZB11 and ZB31 fluorozirconate glasses (monitored at 14 300 $cm^{-1}$).

### C. FLN emission spectra

An excitation with a narrow line by a tunable laser is known to give narrower emission spectra than a broadband excitation for glassy materials because of the limitation of the excitation in an excitation spectrum broadened by the random distribution of the structure. This method is referred to as FLN and has been used by many spectroscopists investigating rare-earth doped glasses to provide clearer information for the spectra than broadband excitation does.[9,25,26]

Figure 4 shows the simulated (a) and observed (b) FLN emission spectra of $Eu^{3+}$ in the ZB11 and ZB31 glasses. The $^7F_0-^5D_0$ excitation energy was varied for the observed spectra by tuning the excitation laser. A corresponding change of the excitation energy in the simulation was performed grouping the structural models with the $^7F_0-^5D_0$

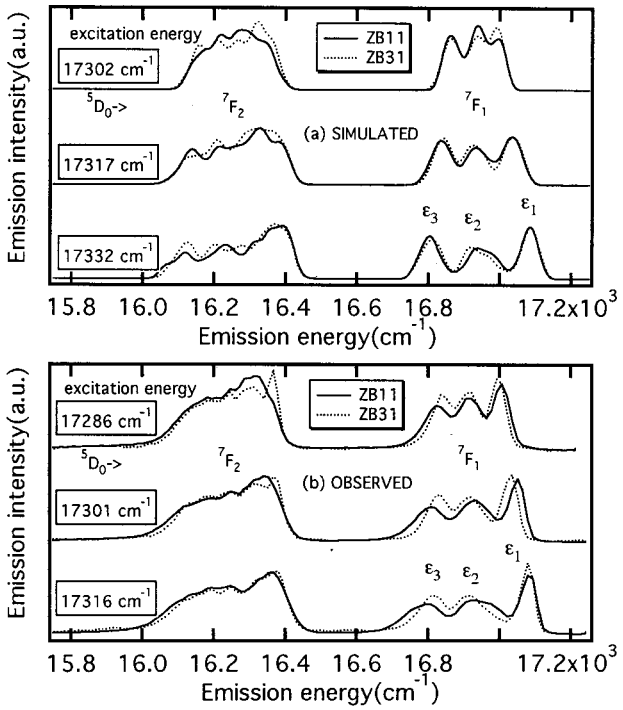


FIG. 4. Simulated (a) and observed (b) FLN emission spectra of $Eu^{3+}$ in ZB11 and ZB31 glasses.

energies in the same region, for example, between 17310 and 17324 $cm^{-1}$, when the simulated emission lines were integrated.

The characteristic differences between the two glasses, which were not clear in the broadband spectra, are clearly observed in the FLN spectra. A gradual increase of the splitting by increasing the excitation energy was observed in the simulated spectra as well as in the observed spectra.

As a matter of convenience, three peaks of the $^5D_0-^7F_1$ band are noted as $\epsilon_1$, $\epsilon_2$, and $\epsilon_3$ from the higher energy side as shown in Fig. 4. The characteristic differences between the ZB11 and ZB31 glasses in the observed spectra were as follows;

(1) In the $^5D_0-^7F_1$ band, the splitting of the $\epsilon_2$ and $\epsilon_3$ components was larger for the ZB11 glass than for the ZB31 glass.
(2) In the $^5D_0-^7F_2$ band, the shoulder on the higher energy side was sharper for the ZB31 glass than for the ZB11 glass.
(3) In the $^5D_0-^7F_2$ band, the differences in the spectral shape and intensity between the two glasses were smaller at the higher excitation energy side of the band.

The above three characteristic differences between the two glasses were reproduced in the simulated spectra. This fact means that the structural difference which affects the spectroscopic character of rare-earth ions in glass was simulated properly by MD simulation, and that the simulation of spectra using a point charge crystal field is usable in analyzing the spectra of the RE ions in glass.

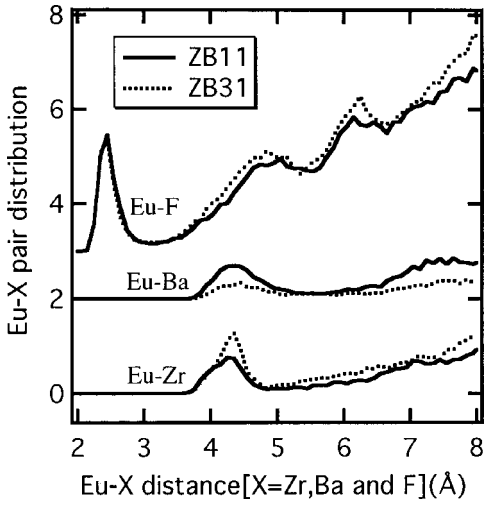


FIG. 5. Pair radial distribution function of Eu–X (X=Zr, Ba, and F) pairs in ZB11 and ZB31 fluorozirconate glasses.

### D. Structure models by MD simulation

The results of optical spectrum simulation showed that the structures of the RE sites, which affected the optical spectra, were reproduced by MD simulation. We will discuss the structural aspects of the RE coordination in the structural models by MD simulation in this section. Figures 5 and 6 show the Eu–X (X=Zr, Ba, and F) pair distributions and cumulative distribution, respectively, as a result of MD simulation. The peak of the Eu–F pair distribution was at 2.4 Å, whose value was comparable with the average Eu–F distances of europium fluoride crystals. The average coordination numbers of the atoms to the Eu ions, obtained from Fig. 6, are shown in Table IV. The Eu–F coordination number was larger in the ZB11 glass than in the ZB31 glass. Comparing $R_N$=N(Ba)/N(Zr+Ba) (ratio of the number of atoms in a cell) with $R_{NC}=N_C$(Eu–Ba)/$N_C$(Eu–{Zr+Ba}) (the ra-

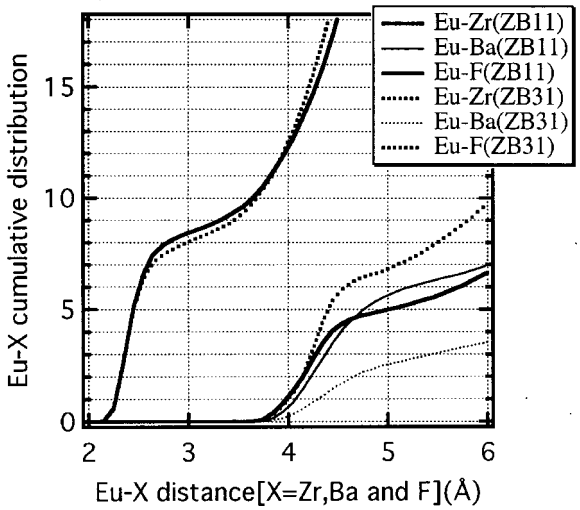


FIG. 6. Eu–X (X=Zr, Ba, and F) cumulative distribution of ZB11 and ZB31 fluorozirconate glasses.

TABLE IV. Average coordination numbers of atoms to europium ions.

| | | Size of the coordination | ZB11 | ZB31 |
|---|---|---|---|---|
| Average coordination number | $N_c$(Eu–F) | 3.2 | 8.8 | 8.4 |
| | $N_c$(Eu–Zr) | 5.5 | 5.6 | 8.0 |
| | $N_c$(Eu–Ba) | 5.5 | 6.3 | 3.1 |
| Ratio of coordination number of cations to a europium ion | $R_{NC}=N_c$(Eu–Ba)/ $N_c$(Eu–{Zr+Ba}) | | 0.53 | 0.28 |
| Ratio of the number of cations in a unit cell | $R_N$=N(Ba)/ N(Zr+Ba) | 0.50 | | 0.25 |

tio of coordination numbers), the $R_{NC}$ was larger in both ZB11 and ZB31. Thus barium atoms tended to coordinate to $EuF_x$ polyhedron in both glasses.

## V. CONCLUSION

The simulation of the spectra of $Eu^{3+}$-doped fluorozirconate glasses with two compositions, Zr:Ba=1:1 (ZB11) and Zr:Ba=3:1 (ZB31), was studied using MD simulations and a point charge crystal field. The characteristic differences of observed emission spectra between two glasses were revealed as sharper profiles of the peaks of the ZB31 glass compared with those of the ZB11 glass. A difference in the splitting behavior between the two glasses by the change of excitation energy was observed for the FLN emission spectra. Those differences in the observed optical spectra were reproduced in the simulated spectra. The analysis of structural models by MD simulation showed that barium ions tended more to coordinate with $EuF_a$ clusters than with zirconium ions.


[1] R. Reisfeld and C. K. Jorgensen, *Handbook on the Physics and Chemistry of Rare Earths*, edited by K. A. Gschneidner and L. Eyring (1987), Chap. 58, pp. 1–90.
[2] J. Lucas and J. Adam, Glastech. Ber. **62**, 422 (1989).
[3] M. Yamada, T. Kanamori, Y. Terunuma, K. Okawa, M. Shimizu, S. Sudo, and K. Sagawa, IEEE Photonics Technol. Lett. **8**, 882 (1996).
[4] R. C. Powell, *Physics of Solid-State Laser Materials* (Springer, New York, 1998).
[5] S. Hufner, *Optical Spectra of Transparent Rare Earth Compounds* (Academic, New York, 1978).
[6] G. H. Dieke, *Spectra and Energy Levels of Rare Earth Ions in Crystals* (Interscience, New York, 1968).
[7] B. R. Judd, Phys. Rev. **127**, 750 (1962).
[8] G. S. Ofelt, J. Chem. Phys. **37**, 511 (1962).
[9] K. Soga, M. Uo, H. Inoue, and A. Makishima, J. Am. Ceram. Soc. **78**, 129 (1995).
[10] K. Soga, H. Inoue, A. Makishima, and S. Inoue, Phys. Chem. Glasses **36**, 253 (1995).
[11] P. Porcher and P. Caro, J. Chem. Phys. **65**, 89 (1976).
[12] P. Porcher and P. Caro, J. Chem. Phys. **68**, 4176 (1978).
[13] P. Porcher and P. Caro, J. Chem. Phys. **68**, 4183 (1978).
[14] P. Porcher and P. Caro, J. Lumin. **21**, 207 (1980).
[15] M. Taibi, J. Aride, E. AnticFidancev, M. LemaitreBlaise, and P. Porcher, Phys. Status Solidi A **115**, 523 (1989).
[16] E. Anticfidancev, M. LemaitreBlaise, P. Porcher, M. Taibi, and J. Aride, J. Alloys Compd. **188**, 75 (1992).
[17] E. AnticFidancev, J. Aride, M. LemaitreBlaise, P. Porcher, and M. Taibi, J. Alloys Compd. **188**, 242 (1992).
[18] C. Cascales, E. AnticFidancev, M. LemaitreBlaise, and P. Porcher, J. Alloys Compd. **180**, 111 (1992).
[19] E. AnticFidancev, M. LemaitreBlaise, J. Chaminade, and P. Porcher, J. Alloys Compd. **180**, 223 (1992).
[20] E. AnticFidancev, C. Cascales, M. LemaitreBlaise, and P. Porcher, J. Alloys Compd. **207**, 178 (1994).
[21] A. Florez, M. Florez, S. A. LopezRivera, J. Martin, P. Porcher, O. L. Malta, Y. Messaddeq, and M. A. Aegerter, J. Alloys Compd. **275–277**, 333 (1998).
[22] J. Holsa, R. J. Lamminmaki, and P. Porcher, J. Alloys Compd. **275–277**, 398 (1998).
[23] J. Holsa, E. Sailynoja, P. Ylha, E. AnticFidancev, M. LemaitreBlaise, and P. Porcher, J. Chem. Soc., Faraday Trans. **94**, 481 (1998).
[24] J. Holsa, R. J. Lamminmaki, P. Porcher, P. Deren, and W. Strek, Spectrochim. Acta, Part A **54**, 2189 (1998).
[25] C. Brecher and L. A. Riseberg, Phys. Rev. B **13**, 81 (1976).
[26] C. Brecher and L. A. Riseberg, Phys. Rev. B **21**, 2607 (1980).
[27] S. A. Brawer and M. J. Weber, Appl. Phys. Lett. **35**, 31 (1979).
[28] S. A. Brawer and M. J. Weber, Phys. Rev. Lett. **45**, 460 (1980).
[29] S. Brawer and M. J. Weber, J. Non-Cryst. Solids **38&39**, 9 (1980).
[30] M. J. Weber and S. A. Brawer, J. Non-Cryst. Solids **52**, 321 (1982).
[31] G. Cormier and J. A. Capobianco, Europhys. Lett. **24**, 743 (1993).
[32] G. Cormier, J. A. Capobianco, C. A. Morrison, and A. Monteil, Phys. Rev. B **48**, 16290 (1993).
[33] G. Cormier, J. A. Capobianco, and C. A. Morrison, J. Chem. Soc., Faraday Trans. **90**, 755 (1994).
[34] M. T. Harrison and R. G. Deaning, J. Lumin. **69**, 265 (1996).
[35] A. Monteil, S. Chaussedent, and J. A. Capobianco, Mol. Simul. **20**, 127 (1997).
[36] H. Inoue, K. Soga, and A. Makishima, J. Non-Cryst. Solids **222**, 212 (1997).
[37] W. T. Carnall, P. R. Fields, and K. Ra Jnak, J. Chem. Phys. **46**, 4450 (1968).
[38] H. Adachi, M. Tsukada, and C. Satoko, J. Phys. Soc. Jpn. **45**, 875 (1978).
[39] W. Krupke, Phys. Rev. **145**, 325 (1966).